Mineralogical Magazine, October 2015, Vol. 79(5), pp. 1073–1087

New minerals with a modular structure derived from hatrurite from the pyrometamorphic Hatrurim Complex. Part II. Zadovite, $BaCa_6[(SiO_4)(PO_4)](PO_4)_2F$ and aradite, $BaCa_6[(SiO_4)(VO_4)](VO_4)_2F$, from paralavas of the Hatrurim Basin, Negev Desert, Israel

E.V. Galuskin[1,*], F. Gfeller[2], I.O. Galuskina[1], A. Pakhomova[2], T. Armbruster[2], Y. Vapnik[3], R. Włodyka[1], P. Dzierżanowski[4] and M. Murashko[5]

[1] Faculty of Earth Sciences, Department of Geochemistry, Mineralogy and Petrography, University of Silesia, Będzińska 60, 41-200 Sosnowiec, Poland
[2] Mineralogical Crystallography, Institute of Geological Sciences, University of Bern, Freiestrasse 3, CH-3012 Bern, Switzerland
[3] Department of Geological and Environmental Sciences, Ben-Gurion University of the Negev, POB 653, Beer-Sheva 84105, Israel
[4] Institute of Geochemistry, Mineralogy and Petrology, Warsaw University, al. Żwirki i Wigury 93, 02-089 Warsaw, Poland
[5] Saint Petersburg State University, Faculty of Geology, 7-9 Universitetskaya nab., St Petersburg, 199034, Russia

[*Received 6 November 2014; Accepted 20 January 2015; Associate Editor: S.J. Mills*]

ABSTRACT

Zadovite, $BaCa_6[(SiO_4)(PO_4)](PO_4)_2F$ ($R\bar{3}m$, $a = 7.0966(1)$ Å, $c = 25.7284(3)$, $V = 1122.13(3)$ Å^3, $Z = 3$) and aradite, $BaCa_6[(SiO_4)(VO_4)](VO_4)_2F$ ($R\bar{3}m$, $a = 7.1300(1)$, $c = 26.2033(9)$ Å, $V = 1153.63(6)$ Å^3, $Z = 3$) are two new mineral species of a novel modular structure type related closely to the structure of nabimusaite, $KCa_{12}(SiO_4)_4(SO_4)_2O_2F$. Both minerals occur in paralavas enclosed in pyrometamorphic rocks of the Hatrurim Complex, Negev desert, Israel. Zadovite and aradite are colourless, transparent with a white streak, have a vitreous lustre and an uneven fracture. Both minerals are uniaxial (–) with refractive indices (589 nm) $\omega = 1.711(2)$, $\varepsilon = 1.708(2)$ (zadovite) and $\omega = 1.784(3)$, $\varepsilon = 1.780(3)$ (aradite). The zadovite structure type comprises two tetrahedral sites, which may host a broad compositional range of atoms such as Si, P, V and S. Results of electron microprobe analyses show a correlation between excess Si^{4+} and S^{6+} contents, suggesting the substitution scheme $2(P,V)^{5+} = Si^{4+} + S^{6+}$ at the tetrahedral sites. This points to the possibility of new minerals isostructural with zadovite with end-member formulae $BaCa_6(SiO_4)_2[(PO_4)(SO_4)]F$, $BaCa_6(SiO_4)_2[(VO_4)(SO_4)]F$, $BaCa_6[(SiO_4)_{1.5}(SO_4)_{0.5}](PO_4)_2F$ and $BaCa_6[(SiO_4)_{1.5}(SO_4)_{0.5}](VO_4)_2F$. The Raman spectra of aradite and zadovite reflect the varying PO_4 (e.g. change of band intensity at ~1031 cm^{-1}) and VO_4 contents (e.g. change of band intensity at ~835 cm^{-1}). The presence of SO_4 leads to an additional Raman band at ~997 cm^{-1}. The structure of zadovite-series minerals belonging to the nabimusaite group is characterized by a 1:1 alternation of antiperovskite-like $\{[FCa_6](TO_4)_2\}^{4+}$ modules and $Ba(TO_4)_2^{4-}$ modules.

Keywords: zadovite, aradite, new minerals, modular structure, antiperovskite structure, Raman spectroscopy, Hatrurim Complex, Israel.

* E-mail: evgeny.galuskin@us.edu.pl
DOI: 10.1180/minmag.2015.079.5.04

Introduction

Two new minerals zadovite, $BaCa_6[(SiO_4)(PO_4)](PO_4)_2F$ ($R\bar{3}m$, $a = 7.0966(1)$ Å, $c = 25.7284(3)$, $V = 1122.13(3)$ Å^3, $Z = 3$) and aradite, $BaCa_6[(SiO_4)(VO_4)](VO_4)_2F$ ($R\bar{3}m$, $a = 7.1300(1)$, $c = 26.2033(9)$ Å, $V = 1153.63(6)$ Å^3, $Z = 3$), representing two end-members of the solid solution $BaCa_6[(SiO_4),(PO_4),(VO_4)]_4F$, were discovered in small paralava veins in gehlenite-rich pyrometamorphic rocks of the Hatrurim Complex, Gurim Anticline, Hatrurim Basin (31°12′N 35°14′E), located near the town of Arad in the Negev Desert, Israel.

Zadovite (IMA2013-031) and aradite (IMA2013-047), approved by the International Mineralogical Association Commission on New Minerals, Nomenclature and Classification (IMA-CNMNC) in 2013, are characterized by modular structures (Ferraris et *al*., 2008) and form, together with nabimusaite, $KCa_{12}(SiO_4)_4(SO_4)_2O_2F$ ($R\bar{3}m$, $a = 7.1905(4)$, $c = 41.251(3)$ Å, $V = 1847.1(2)$ Å^3, $Z = 3$) (Galuskin *et al*., 2015*b*), the nabimusaite group. Zadovite and aradite represent a new structure type of this group characterized by intercalation of single $\{[FCa_6](TO_4)_2\}^{4+}$ antiperovskite layers with single $Ba(PO_4)_2^{4-}$ layers, where T = Si, P and V (structure type 1:1, zadovite series). For comparison, nabimusaite is characterized by triple antiperovskite layers $\{[O_2FCa_{12}](SiO_4)_4\}^{3+}$ and intercalated single $K(SO_4)^{3-}$ layers (structure type 3:1, nabimusaite series). Synthetic analogues of zadovite and aradite are not known.

The name zadovite is in honour of the famous Russian mineralogist Aleksandr Efimovich Zadov (1958–2012), author and co-author of more than 90 new mineral species. Aradite is named after the town of Arad near the type locality. Type material is deposited in the mineralogical collections of the Museum of Natural History in Bern, Bernastrasse 5, CH-3005 Bern, Switzerland, catalogue numbers NMBE 42103 (zadovite, the same type specimen is also the holotype for gurimite, IMA2013-032) and NMBE 42188 (aradite). The methods used for the investigations of the zadovite-group minerals are analogous to those of nabimusaite reported by Galuskin *et al*. (2015*b*).

Occurrence and description

Zadovite and aradite were found in the central part of the Hatrurim Basin, ~5 km southeast of the town of Arad, Negev Desert, Israel, one of the most important localities of the pyrometamorphic Hatrurim Complex (Bentor, 1960; Gross, 1977). The Hatrurim Basin is the type locality for bayerite, bentorite, ye'elimite, grossite, hatrurite and nagelschmidtite (Gross, 1977; Vapnik *et al*., 2006). More recently barioferrite, $BaFe_{12}^{3+}O_{19}$ (Murashko *et al*., 2010), murashkoite, FeP, negevite, NiP_2, halamishite, Ni_5P_4, transjordanite, Ni_2P, zuktamrurite, Ni_5P_4 (Britvin *et al*., 2013*a*–*e*), gurimite, $Ba_3(VO_4)_2$ and khesinite, $Ca_4(Mg_3Fe_9^{3+})O_4(Fe_9^{3+}Si_3)O_{36}$ (Galuskina *et al*., 2013, 2014*a*), shulamitite $Ca_3TiFeAlO_8$ (Sharygin *et al*., 2013), fluorkyuygenite $Ca_{12}Al_{14}O_{32}[(H_2O)_4F_2]$ (Galuskin *et al*., 2015*a*) were described. Nabimusaite $KCa_{12}(SiO_4)_4(SO_4)_2O_2F$ was discovered in pyrometamorphic larnite rocks of the Hatrurim Complex on the Jabel Harmun, Judean Mountains, the West Bank, Palestinian Autonomy (Galuskin *et al*., 2015*b*), which is also the type locality for harmunite, vapnikite and dzierżanowskite (Galuskin *et al*., 2014; Galuskina *et al*., 2014*b*,*c*).

Pyrometamorphic rocks of the Hatrurim Complex are highly unusual and formed as alteration products of a high-temperature combustion process. Several researchers consider that high-temperature alteration took place due to combustion of organic matter contained in the sedimentary protolith (Matthews and Gross, 1980; Geller *et al*., 2012). More recent hypotheses discuss methane ignition of gases released by active tectonic zones, analogous to mud volcanism (Sokol *et al*., 2007, 2008; Novikov *et al*., 2013).

Grains of zadovite and aradite only occur within small veins (a few centimetres thick) of schorlomite-rankinite-pseudowollastonite-gehlenite paralavas in fine-grained gehlenite-larnite rocks (Fig. 1). These minerals are generally confined to coarse-grained rankinite and often occur together (Figs 2 and 3). There are three main types of occurrence of minerals of the zadovite–aradite series: (1) grains up to 100–200 µm grew on apatite or are enclosed by its box-like crystals – replacement of apatite by zadovite is also observed; (2) xenomorphic grains 50–100 µm in size developed in the cracks of rankinite and gehlenite; (3) small grains of zadovite–aradite not exceeding 10–15 µm in size in ellipsoidal aggregates of fine-grained Ba-bearing minerals (barite, barioferrite, gurimite, walstromite and fresnoite), kalsilite and wollastonite; these are strongly altered to secondary Ca hydrosilicates. Occasionally, Cu minerals like cuprite and delafossite (Fig. 2*e*) form aggregates

FIG. 1. Small veins of coarse crystalline paralava in gehlenite rock. Minerals in the paralava are distinguished by colour. Schorlomite and Ti-rich andradite – black, dark-brown; gehlenite – brown, yellow-brown; rankinite, pseudowollastonite, fluorapatite, cuspidine – light-brown, pink, light-grey; secondary Ca-hydrosilicates – chalk white.

together with kalsilite. Compared to zadovite, aradite is relatively rare. Platy zadovite crystals with well-developed {001} forms and xenomorphic crystals are observed (Figs 2*b* and *e*).

Aradite and zadovite are associated with the rock-forming minerals gehlenite (often with high concentrations of Fe^{3+}, Mg and Na impurities), pseudowollastonite and wollastonite, garnet-supergroup minerals of the andradite–schorlomite series, rankinite, magnesioferrite (enriched in Cu, Ni and Mn), kalsilite and fluorapatite. Less frequent associates are P-rich ellestadite, larnite, cuspidine and hematite. The host rocks of the new mineral also display striking eutectic intergrowths of schorlomite or gehlenite with a larnite-like phase on the microscopic level. The larnite-like phase was originally described by Gross (1977) as nagelschmidtite, forming colonies of chimney-like crystals growing sub-perpendicular to garnet and gehlenite growth zones. This phase was approved recently by the IMA-CNMNC as flamite (IMA2013-122) with formula $(Ca,Na,K)_2(Si,P)O_4$ [$P6_3$, $a = 43.373(2)$, $c = 6.8270(4)$ Å] (Sokol *et al*., 2014), but according to our data (Gfeller *et al*., 2015) the structure corresponds to a cyclic twin of the known synthetic orthorhombic phase 'α'-Ca_2SiO_4' (Saalfeld and Klaska, 1981; Mumme *et al*., 1995). Accessory minerals are represented by dorrite–khesinite, barioferrite, walstromite, barite, gurimite, fresnoite, delafossite, cuprite, vorlanite, perovskite and 'hexacelsian'. The mineral content of the fine-grained gehlenite host rocks is not so complex, mainly comprising gehlenite, larnite, magnesioferrite and andradite.

Zadovite and aradite are colourless, transparent with a white streak, have vitreous lustre and uneven fracture. Both minerals are uniaxial (-) with refractive indices (589 nm) $\omega = 1.711(2)$, $\varepsilon = 1.708(2)$ (zadovite) and $\omega = 1.784(3)$, $\varepsilon = 1.780(3)$ (aradite). UV fluorescence was not observed. Microhardness was only measured for zadovite, which at a 50 g load varies from 532 to 634 kg mm^{-2}, with a mean of 564 kg mm^{-2} (for 12 measurements). This value corresponds to a Mohs' hardness of ~5–5½. The density of zadovite and aradite could not be measured directly because of small grain size and chemical variability. Calculated densities derived from the empirical formulae are 3.503 g cm^{-3} for zadovite and 3.509 g cm^{-3} for aradite.

Chemical composition, Raman spectroscopy studies and crystal structures of zadovite and aradite

Minerals of the zadovite–aradite series are characterized by significant variations in composition (Table 1). The vanadium content in zadovite, which has a V-free end-member formula, is never lower than 2–3 wt.% of V_2O_5 (Table 1, analyses 1 and 3). The maximum V content in aradite is 24.7 wt.% V_2O_5 with ≈ 4.5 wt.% P_2O_5 (Table 1, analysis 4). Aradite grains <3 μm in size contain according to energy dispersive spectroscopy contain ~28 wt.% V_2O_5 (~2.57 V per formula unit (p.f.u.)) and 1.5 wt.% P_2O_5 (~0.17 P p.f.u.). For these grains Raman spectra were collected (Fig. 4).

Intermediate compositions between aradite and zadovite are characteristic of many analysed crystals (Table 1, analysis 5). Occasionally, a tendency to vanadium enrichment in late aradite–zadovite zones is observed. Minor sulfate (1–2 wt.% SO_4) is generally present. The Si content (>1 a.p.f.u.) is higher than the maximum content defined by the crystal-chemical formula (Table 1). In one case an aggregate of zadovite–aradite grains up to 50 μm in size was detected; some of those crystals were enriched in Si and S (Table 1, analysis 6).

Crystals of the zadovite–aradite series are characterized by variable V_2O_5 contents leading to different intensities of Raman bands (Fig. 4). In addition, a spectrum of an aradite-like phase with

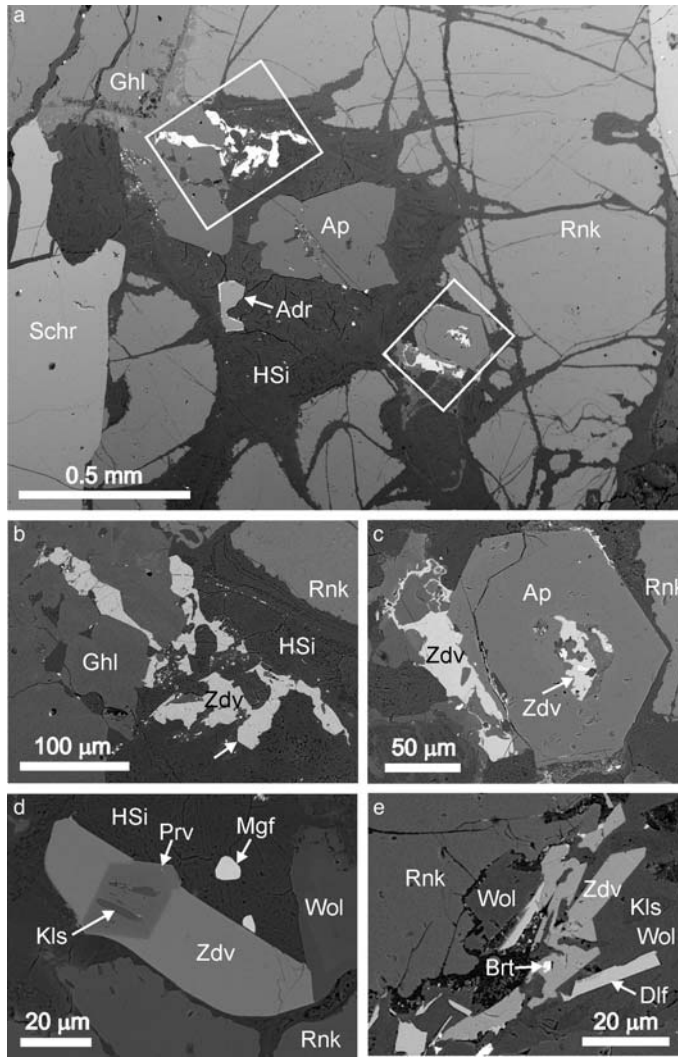

FIG. 2. Backscattered electron (BSE) images of zadovite in paralava from the Gurim anticline: (*a*) Zadovite grown on fluorapatite or occupying cracks in rock-forming minerals. Framed sections are magnified in (*b*) and (*c*). (*b*) Xenomorphic aggregates of zadovite. (*c*) Zadovite enclosed in box-like apatite and growing on apatite. (*d*, *e*) Tabular zadovite crystals with developed {001} faces and small rhombohedral faces. Adr = Ti-bearing andradite, Ap = fluorapatite, Brt = barite, Dlf = delafossite, Ghl = gehlenite, HSi = undiagnosed Ca hydrosilicates, Kls = kalsilite, Mgf = magnesioferrite, Prv = perovskite, Rnk = rankinite, Schr = schorlomite, Wol = pseudowollastonite, Zdv = zadovite.

anomalously high contents of SiO_2 and SO_3 (Fig. 4) has been collected. The main bands in the Raman spectra of the zadovite-group minerals are related to vibrations of the (TO_4) tetrahedral groups, PO_4^{3-}, VO_4^{3-}, SiO_4^{4-} and SO_4^{2-} (Fig. 4). Bands from symmetric (ν_1) and antisymmetric (ν_3) stretching vibrations of (TO_4) occur above 800 cm^{-1}, bands in the range 300–700 cm^{-1} are attributed to bending vibrations (ν_2 and ν_4), bands below 300 cm^{-1} are assigned to stretching vibrations of Ca–O and also the vibration of R(TO_4) and T(TO_4) (Comodi *et al.*, 1999; Frost *et al.*, 2007, 2011). Raman spectra of the zadovite-group minerals were normalized to the intensity of the main $\nu_1(SiO_4^{4-})$ band at ~860 cm^{-1} (Fig. 4). Bands from stretching vibrations of VO_4^{3-} and SiO_4^{4-} partially overlap. This makes it difficult

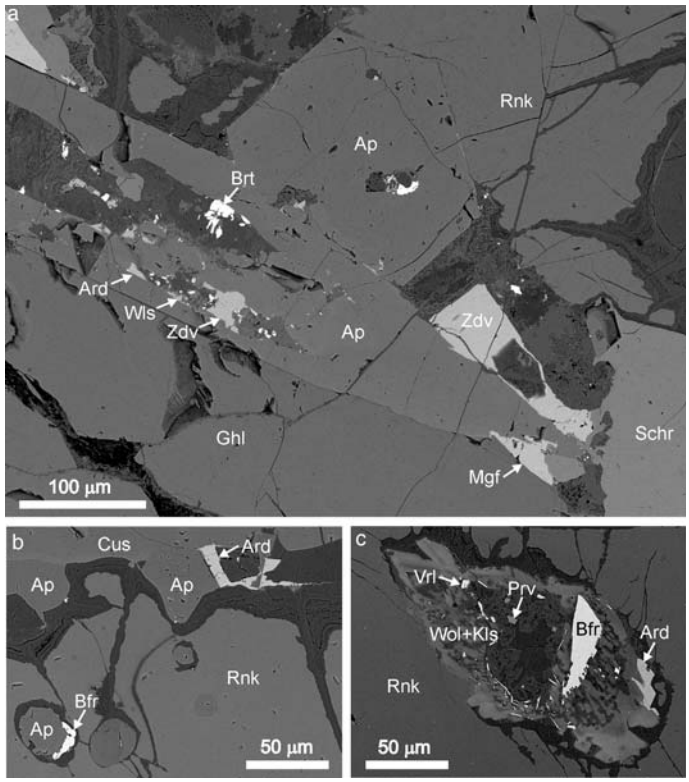

FIG. 3. BSE images of zadovite–aradite paragenesis: (*a*) Aradite in association with zadovite, high-vanadian phases of zadovite-aradite are rare and are characterized by a smaller crystal size. (*b*) Aradite crystal used for structural and Raman studies. (*c*) Small kalsilite-wollastonite inclusions enriched in Ba minerals surrounded by rankinite. Ap = fluorapatite, Ard = aradite, Bfr = barioferrite, Brt = barite, Cus = cuspidine, Ghl = gehlenite, Kls = kalsilite, Mgf = magnesioferrite, Prv = perovskite, Rnk = rankinite, Schr = schorlomite, Wol = psewdowollastonite, Wls = walstromite, Vrl = vorlanite, Zdv = zadovite.

to use them for distinguishing between zadovite and aradite. The split $\nu_1(PO_4)^{3-}$ band does not allow a determination of zadovite and aradite, but indicates that P partially occupies two different tetrahedral sites. The band near 950 cm^{-1} is related to the *T*2 site, and that at 970 cm^{-1} corresponds to *T*1 (see structure description below). This band assignment is confirmed by the Raman spectrum of S-rich aradite, where the *T*1 site is fully occupied by Si (1.84 p.f.u.); thus P resides at *T*2, leading to only one $\nu_1(PO_4)^{3-}$ Raman band at ~950 cm^{-1}. In Raman spectra of the zadovite-group minerals no splitting of the $\nu_1(SiO_4)^{4-}$ band is observed. However, splitting of this band is characteristic of the nabimusaite spectrum and indicates Si incorporation at two different tetrahedral sites (Galuskin *et al*., 2015*b*).

A grain of zadovite, 150 µm × 60 µm × 60 µm in size, was used for the single-crystal X-ray structure study. The aradite structure was refined from a grain selected from a thin section shown by an arrow in Fig. 3*b*. This 30 µm ×20 µm ×10 µm grain was intergrown with wollastonite (Fig. S1, supplementary materials which have been deposited with the Principal Editor of *Mineralogical Magazine* and are available from www.minersoc.org/pages/e_journals/dep_mat_mm.html). Experimental details and results of the single-crystal X-ray studies are summarized in Tables 2–5. Crystal-chemical formulae of zadovite and aradite are $BaCa_6[(SiO_4)(PO_4)][(PO_4)_{1.39}(VO_4)_{0.61}]F$ and $BaCa_6[(Si,P)O_4)_{1.53}(VO_4)_{0.47}][(VO_4)_{1.51}(PO_4)_{0.49}]F$, respectively. Refined electron numbers ~63.9 (zadovite) and ~74.4 e^- (aradite) for tetrahedral sites

TABLE 1. Composition of zadovite–aradite series, wt.%.

	zadovite (zdv)			aradite (ard)			zdv	ard	'ard-P'	'zadovite–aradite-S'			ard
		1			2		3	4	5		6		7
	Mean (n = 14)	S.D.	Range	Mean (n = 5)	S.D.	Range				Mean (n = 5)	S.D.	Range	
SO_3	1.22	0.12	0.98–1.37	1.58	0.51	0.84–2.22	1.34	0.84	1.87	8.45	0.17	2.03–2.45	1.35
CrO_3	<0.08			<0.08			<0.08	<0.08	<0.08	<0.08			0.22
V_2O_5	7.51	0.86	6.20–9.07	22.09	2.09	19.95–24.69	2.45	24.69	12.67	6.76	1.83	5.61–10.40	14.99
P_2O_5	19.29	0.85	17.49–20.57	5.46	1.28	3.77–7.01	22.65	4.49	12.62	6.39	1.78	5.14–9.79	8.56
SiO_2	8.43	0.07	8.28–8.57	8.79	0.65	7.71–9.50	8.54	7.71	9.40	13.92	1.47	11.07–15.00	11.30
Fe_2O_3	<0.08			0.10	0.05	0.03–0.18	<0.08		<0.08	0.13	0.05	0.09–0.22	0.19
Al_2O_3	<0.03			0.03	0.02	0.00–0.06	<0.03		<0.03	<0.03			<0.03
CaO	42.26	0.20	41.89–42.57	40.80	0.17	40.53–40.99	42.20	40.05	41.62	42.22	0.29	41.70–42.49	41.36
BaO	19.92	0.20	19.58–20.28	18.24	0.37	18.09–18.79	19.50	18.50	19.26	19.50	0.34	18.91–19.88	19.66
SrO	0.33	0.04	0.24–0.38	0.32	0.08	0.22–0.42	0.30	0.42	0.36	0.42	0.07	0.37–0.55	0.50
Na_2O	0.18	0.02	0.16–0.21	0.05	0.03	0.02–0.11	0.23	0.11	0.07	<0.02			<0.02
F	2.45	0.13	2.21–2.77	2.36	0.07	2.31–2.49	2.41	2.49	2.38	2.38	0.17	2.13–2.54	2.52
H_2O													0.43
–O = F	1.03			0.99			1.01	1.05	1.00	1.00			1.06
Total	100.56			98.84			98.61	98.24	99.24	99.18			100.02
Calculated on 17(O + F)													
Ba	1.02			0.98			1.01	1.01	1.01	1.01			1.03
Ca	5.91			5.99			5.95	5.98	5.98	5.98			5.94
Sr	0.02			0.02			0.02	0.03	0.02	0.03			0.04
Na	0.05			0.01			0.06	0.03	0.02				
Sum $A + X$	7.00			7.00			7.04	7.05	7.03	7.02			7.01
Si	1.10			1.20			1.12	1.07	1.26	1.84			1.51
P	2.13			0.63			2.52	0.53	1.43	0.72			0.97
S^{6+}	0.12			0.16			0.13	0.09	0.19	0.84			0.14
V^{5+}	0.65			2.00			0.21	2.27	1.12	0.59			1.33
Al				0.01									
Cr^{6+}													0.02
Fe^{3+}				0.01						0.01			0.02
Sum $T1 + T2$	4.00			4.01			3.98	3.96	4.00	4.00			3.99
OH													0.38
F	1.01			1.02			1.00	1.10	1.01	0.99			1.07

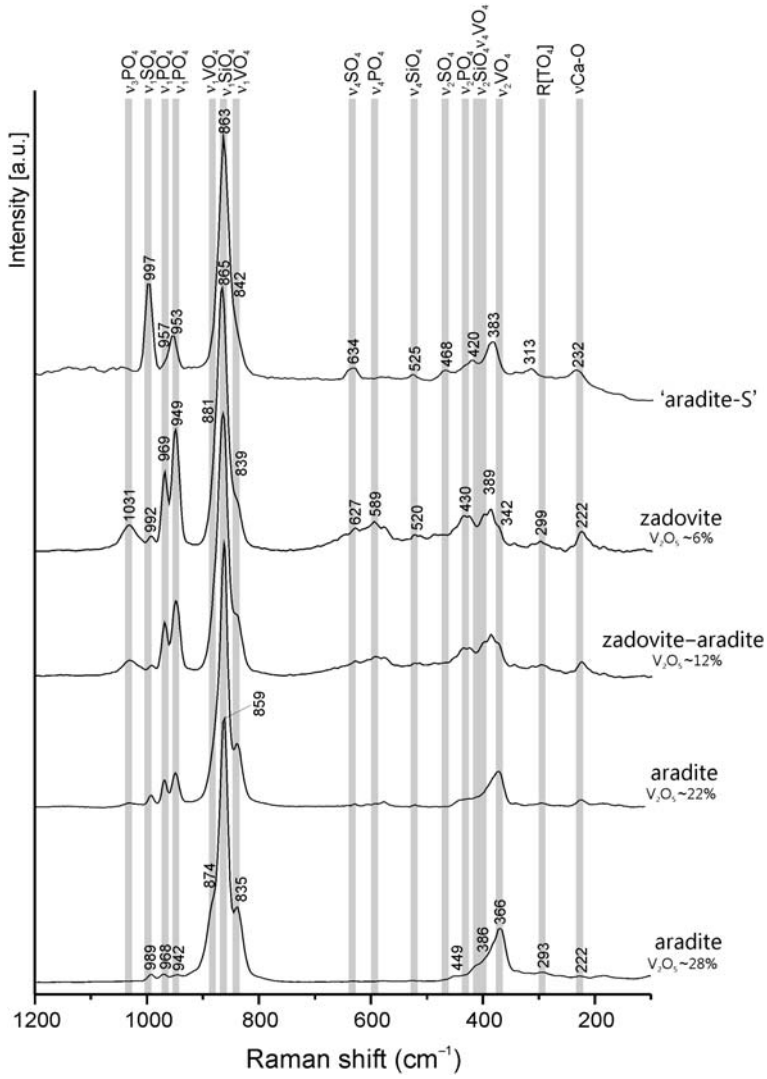

FIG. 4. Raman spectra of the zadovite–aradite series minerals.

correspond to values calculated from electron microprobe analysis (EMPA) data: 64.22 (zadovite) and 75.2 e^- (aradite) (Table 1). Silicon, P, S and Al cannot be distinguished by their scattering behaviour. Thus for proper assignment refined electron numbers at the tetrahedral sites *T1* and *T2* were corroborated by differences in *T*–O bond lengths $PO_4^{3-} \approx 1.55$ Å, $SiO_4^{4-} \approx 1.64$ Å, $SO_4^{2-} \approx 1.48$ Å and $VO_4^{3-} \approx 1.73$ Å; mean *T*–O distances are from Dickens and Brown (1971), Sokolova *et al*. (1984), Fayos *et al*. (1985), Irran *et al*. (1997), Schindler *et al*. (2000) and our unpublished data). Thus, the crystal chemical formulae of zadovite and aradite according to the results of EMPA were modified to $Ba_{1.02}(Ca_{5.91}Na_{0.05}Sr_{0.02})_{\Sigma 5.98}[(SiO_4)_{1.10}(PO_4)_{0.78}(SO_4)_{0.12}]_{\Sigma 2}[(PO_4)_{1.35}(VO_4)_{0.65}]_{\Sigma 2}F_{1.01}$ ($T1$–$O_{cal.} \approx 1.60$ Å, $T2$–$O_{cal.} \approx 1.61$ Å) and $(Ba_{0.98}Sr_{0.02})_{\Sigma 1}(Ca_{5.99}Na_{0.01})_{\Sigma 6}[(SiO_4)_{1.20}(VO_4)_{0.49}(PO_4)_{0.14}(SO_4)_{0.16}(AlO_4)_{0.01}]_{\Sigma 2}[(VO_4)_{1.5}(PO_4)_{0.49}(Fe^{3+}O_4)_{0.01}]_{\Sigma 2.01}F_{1.02}$ ($T1$–$O_{cal.} \approx 1.64$ Å, $T2$–$O_{cal} \approx 1.69$ Å), respectively.

Powder X-ray diffraction patterns (Tables S1 and S2, supplementary materials which have been deposited with the Principal Editor of *Mineralogical Magazine* and are available from www.minersoc.org/

TABLE 2. Refinement and data collection parameters for zadovite and aradite.

	zadovite*	aradite*
Crystal data		
Unit-cell dimensions (Å)	$a = 7.0966(1)$	$a = 7.1300(1)$
	$c = 25.7284(3)$	$c = 26.2033(9)$
Space group	$R\bar{3}m$	
Volume (Å^3)	1122.13(3)	1153.63(6)
Z	3	
Intensity measurement		
Crystal shape	prism	prism
Crystal size (mm)	0.15 × 0.06 × 0.06	0.03 × 0.02 × 0.01
Diffractometer	APEX II SMART	
X-ray radiation	Mo$K\alpha$	
X-ray power	50 kV 30 mA	
Monochromator	Graphite	
Temperature	293 K	
Detector to sample distance	5.95 cm	
Measurement method	Phi and Omega scans	
Radiation width	0.5°	
Time per frame	60 s	100 s
Max. θ° range for Data collection	36.25	30.49
Index ranges	$-11 \le h \le 11$	$-9 \le h \le 10$
	$-11 \le k \le 11$	$-9 \le k \le 10$
	$-42 \le l \le 42$	$-35 \le l \le 37$
No. of measured reflections	13288	3625
No. of unique reflections	725	483
No. of observed reflections ($I > 2\sigma(I)$)	705	399
Refinement of the structure		
No. of parameters used in refinement	38	37
R_{int}	0.0202	0.0588
R_σ	0.0072	0.0345
R_1, $I > 2\sigma(I)$	0.0124	0.0304
R_1 all data	0.0129	0.0458
wR_2 on ($F2$)	0.0342	0.0600
Goof	1.169	1.053
Δρ min (e Å^{-3})	–0.53 close to Ca1	–0.82 close to F
Δρ max (e Å^{-3})	0.48 close to Ba1	0.94 close to O4

*For zadovite = $BaCa_6[(SiO_4)(PO_4)][(PO_4)_{1.39}(VO_4)_{0.61}]F$ and aradite = $BaCa_6[((Si,P)O_4)_{1.526}(VO_4)_{0.474}][(VO_4)_{1.512}(PO_4)_{0.488}]F$.

pages/e_journals/dep_mat_mm.html) are calculated from the results of the single-crystal structure refinements.

Discussion

The crystal-chemical formula of holotype zadovite can be simplified to $BaCa_6[(SiO_4)_{1.1}(PO_4)_{0.8}(SO_4)_{0.1}]_{\Sigma 2}[(PO_4)_{1.35}(VO_4)_{0.65}]_{\Sigma 2}F$ leading to the end-member formula $BaCa_6[(SiO_4)(PO_4)](PO_4)_2F$ with double-site occupation at *T1*. The simplified crystal-chemical formula of holotype aradite is $BaCa_6[(SiO_4)_{1.2}(VO_4)_{0.5}(PO_4)_{0.1}(SO_4)_{0.2}]_{\Sigma 2}[(VO_4)_{1.5}(PO_4)_{0.5}]_{\Sigma 2}F$, with the end-member formula $BaCa_6[(SiO_4)(VO_4)](VO_4)_2F$. In the case of the aradite grain studied structurally, *T1* is occupied by V > P. From the chemical composition (EMPA) of holotype aradite for grains without structural data, there is good reason (The ionic radius and electronegativity of P is closer to that of Si than of V) to assign all P to *T*1, $BaCa_6[(SiO_4)_{1.20}(PO_4)_{0.65}(SO_4)_{0.15}]_{\Sigma 2}(VO_4)_2F$, yielding the end-member formula $BaCa_6[(SiO_4)(PO_4)](VO_4)_2F$. Intermediate compositions between aradite and zadovite occur frequently in paralavas of the Hatrurim Complex. Such a chemical composition is given in Table 1 (analysis 5) and refers to the formula $Ba_{1.01}(Ca_{5.98}Na_{0.02}Sr_{0.02})_{\Sigma 6.02}[(SiO_4)_{1.25}(PO_4)_{0.55}(SO_4)_{0.19}]_{\Sigma 1.99}[(VO_4)_{1.12}(PO_4)_{0.88}]_{\Sigma 2}F_{1.01}$. Its Raman spectrum corresponds to the spectrum with 12% V_2O_5 in Fig. 4, suggesting that P is split on two sites. Small amounts of V probably reside at the *T*1 site, but independently to this possible substitution, the end-member formula becomes $BaCa_6[(SiO_4)(PO_4)](VO_4)_2F$, which is another potentially new mineral species.

To solve crystal-chemical problems of the zadovite group we constructed a series of plots using EMPA data (Fig. 5). In the V-P diagram (p.f.u.) there is an obvious linear dependence between V and P defining the isomorphic substitution $V^{5+} \leftrightarrow P^{5+}$ in spite of the different V^{5+} and P^{5+} ionic radii of 0.17 and 0.355 Å, respectively (Shannon, 1976). Probably, complete isomorphism between V^{5+} and P^{5+} is related to the anomalously high temperature of paralava formation (>1200°C), which is supported by the association with pseudowollastonite (Seryotkin *et al*., 2012). Analytical points in the V^{5+} *vs.* P^{5+} diagram (Fig. 5) occupy a broad band. This indicates the potential influence of an additional component in the solid solution different from the formula $BaCa_6[(SiO_4)(R^{5+}O_4)](R^{5+}O_4)_2F$, where

TABLE 3*a*. Atom coordinates and equivalent isotropic displacement parameters (Å^2) for zadovite.

Site	Atom	*x/a*	*y/b*	*z/c*	U_{eq}	Occupancy
*Ba*1	Ba	1/3	2/3	1/6	0.01736(6)	0.9882(18)
	Na				0.01736(6)	0.0117(18)
*Ca*1	Ca	0.839047(19)	0.67809(4)	0.064629(10)	0.01525(7)	1
*T*1	Si	1/3	2/3	0.031394(18)	0.00734(9)	0.50*
	P					0.50*
*T*2	P	2/3	1/3	0.153942(15)	0.00858(11)	0.695(6)
	V					0.305(6)
*O*1	O	1/3	2/3	0.96863(6)	0.0175(3)	1
*O*2	O	0.20896(8)	0.79104(8)	0.04904(4)	0.0220(2)	1
*O*3	O	0.54679(8)	0.09359(16)	0.13074(4)	0.01908(18)	1
*O*4	O	2/3	1/3	0.21668(6)	0.0172(3)	1
*F*1	F	0	0	0	0.0256(4)	1

*Occupancies based on EMPA, charge balance and bond lengths.

TABLE 3*b*. Atom coordinates and equivalent isotropic displacement parameters (Å^2) for aradite.

Site	Atom	*x/a*	*y/b*	*z/c*	U_{eq}	Occupancy
*Ba*1	Ba	1/3	2/3	1/6	0.0228(2)	1
*Ca*1	Ca	0.83980(7)	0.67959(14)	0.06373(4)	0.0145(2)	1
*T*1	Si	1/3	2/3	0.03047(7)	0.0063(5)	0.5*
	P					0.263*
	V					0.237(13)
*T*2	V	2/3	1/3	0.15392(5)	0.0076(4)	0.756(14)
	P			0.15392(5)	0.0076(4)	0.244(14)
*O*1	O	1/3	2/3	0.9675(2)	0.0168(12)	1
*O*2	O	0.2075(3)	0.7925(3)	0.04797(14)	0.0226(8)	1
*O*3	O	0.5426(3)	0.0852(5)	0.12905(12)	0.0189(7)	1
*O*4	O	2/3	1/3	0.2195(2)	0.0151(12)	1
*F*1	F	0	0	0	0.0246(17)	1

*Occupancies based on EMPA, charge balance and bond lengths.

TABLE 4*a*. Anisotropic displacement parameters (Å^2) for zadovite.

Site	U^{11}	U^{22}	U^{33}	U^{23}	U^{13}	U^{12}
*Ba*1	0.01345(7)	0.01345(7)	0.02518(10)	0	0	0.00673(3)
*Ca*1	0.01036(8)	0.00917(10)	0.02583(13)	0.00038(8)	0.00019(4)	0.00459(5)
*T*1	0.00622(12)	0.00622(12)	0.00958(18)	0	0	0.00311(6)
*T*2	0.00947(13)	0.00947(13)	0.00679(16)	0	0	0.00474(6)
*O*1	0.0200(4)	0.0200(4)	0.0124(6)	0	0	0.0100(2)
*O*2	0.0125(3)	0.0125(3)	0.0409(5)	−0.00441(18)	0.00441(18)	0.0062(3)
*O*3	0.0215(3)	0.0149(4)	0.0185(4)	0.0039(3)	0.00193(15)	0.00746(19)
*O*4	0.0163(4)	0.0163(4)	0.0190(6)	0	0	0.0082(2)
*F*1	0.0233(6)	0.0233(6)	0.0301(11)	0	0	0.0117(3)

TABLE 4*b*. Anisotropic displacement parameters (Å^2) for aradite.

Site	U^{11}	U^{22}	U^{33}	U^{23}	U^{13}	U^{12}
*Ba*1	0.0124(2)	0.0124(2)	0.0436(6)	0	0	0.00619(12)
*Ca*1	0.0115(3)	0.0089(4)	0.0223(5)	0.0004(4)	0.00019(19)	0.0044(2)
*T*1	0.0058(6)	0.0058(6)	0.0073(10)	0	0	0.0029(3)
*T*2	0.0091(4)	0.0091(4)	0.0046(7)	0	0	0.0045(2)
*O*1	0.0223(19)	0.0223(19)	0.006(3)	0	0	0.0111(9)
*O*2	0.0127(12)	0.0127(12)	0.041(2)	–0.0037(8)	0.0037(8)	0.0055(13)
*O*3	0.0247(14)	0.0140(16)	0.0143(18)	0.0024(13)	0.0012(6)	0.0070(8)
*O*4	0.0158(17)	0.0158(17)	0.014(3)	0	0	0.0079(8)
F	0.026(2)	0.026(2)	0.023(4)	0	0	0.0128(12)

$R = V^{5+}$ or P. In particular, the substitution $Si^{4+} + S^{6+} = 2(P,V)^{5+}$ contributes to the composition of the solid-solution series. This conclusion is supported by relations seen in $(V + P)^{5+}$ *vs.* S^{6+}, $(V + P)^{5+}$ *vs.* Si^{4+} and Si^{4+} *vs.* S^{6+} diagrams (Fig. 5). In larnite rocks of the Hatrurim Complex three phases of the nabimusaite group containing only S- and Si-tetrahedra are known, nabimusaite, $KCa_{12}(SiO_4)_4(SO_4)_2O_2F$, and the two potential new mineral species, a Ba-analogue of nabimusaite, $BaCa_{12}(SiO_4)_4(SO_4)_2O_3$ (Galuskin *et al.*, 2015*b*) and $BaCa_6(SiO_4)_2(SO_4)_2O$. The latter probably belongs to the zadovite structure type. The calculated formula for a grain with maximum S and Si content is $Ba_{1.01}(Ca_{5.98}Sr_{0.03})_{\Sigma 6.01}[(SiO_4)_{1.84}(R^{5+}O_4)_{0.16}]_{\Sigma 2}[(SO_4)_{0.84-x}(VO_4)_{0.59-y}(PO_4)_{0.56-z}]_{\Sigma 2}F_{0.99}$ ($x + y + z = 0.16$; analysis 6 in Table 1). The general formula of this phase is $BaCa_6(SiO_4)_2[(R^{5+}O_4)(SO_4)]_2F$ with $R^{5+} = V$ or P.

The interpretation remains open about the composition $Ba_{1.03}(Ca_{5.94}Sr_{0.04})_{\Sigma 5.98}[(SiO_4)_{1.51}(S^{6+}O_4)_{0.14}(PO_4)_{0.35}]_{\Sigma 2}[(V^{5+}O_4)_{1.33}(PO_4)_{0.62}(Cr^{6+}O_4)_{0.02}(Fe^{3+}O_4)_{0.02}]_{\Sigma 1.99}F_{1.07}(OH)_{0.38}O_{-0.45}$ (Table 1, analysis 7) of the zadovite-group mineral containing an increased Si content (up to 1.55 a.p.f.u.) and a varying S^{6+} content of ~0.2 a.p.f.u. (Fig. 5). The high Si/S ratio in minerals of the zadovite group may lead to the new end-member $BaCa_6[(SiO_4)_{1.5}(SO_4)_{0.5}][R^{5+}O_4)]_2F$.

The structure of zadovite and aradite are represented by intercalation of antiperovskite type, $\{[FCa_6](TO_4)_2\}^{4+}$ and $Ba(TO_4)_2^{4-}$, layers (Fig. 6). The structure contains two tetrahedral sites located at the 3-fold inversion axis. The *T*1 site

TABLE 5. Selected interatomic distances (Å) for zadovite and aradite.

	zadovite		aradite	
Atom	–atom	distance (Å)	–atom	distance (Å)
Ba1	O3 × 6	2.7819(10)	O3 × 6	2.766(3)
Ca1	O1	2.2851(6)	O1	2.289(2)
	O2 × 2	2.3644(7)	O2 × 2	2.362(2)
	O3 × 2	2.5360(7)	O3 × 2	2.564(2)
	O4	2.3887(10)	O4	2.375(3)
	F1	2.5843(2)	F1	2.5890(9)
	O2	2.9835(12)	O2	2.985(4)
*T*1	O2 × 3	1.5948(10)	O2 × 3	1.621(3)
	O4	1.6147(16)	O1	1.652(6)
Mean		1.600		1.628
*T*2	O3 × 3	1.5898(10)	O3 × 3	1.665(3)
	O4	1.6141(17)	O4	1.718(6)
Mean		1.596		1.678

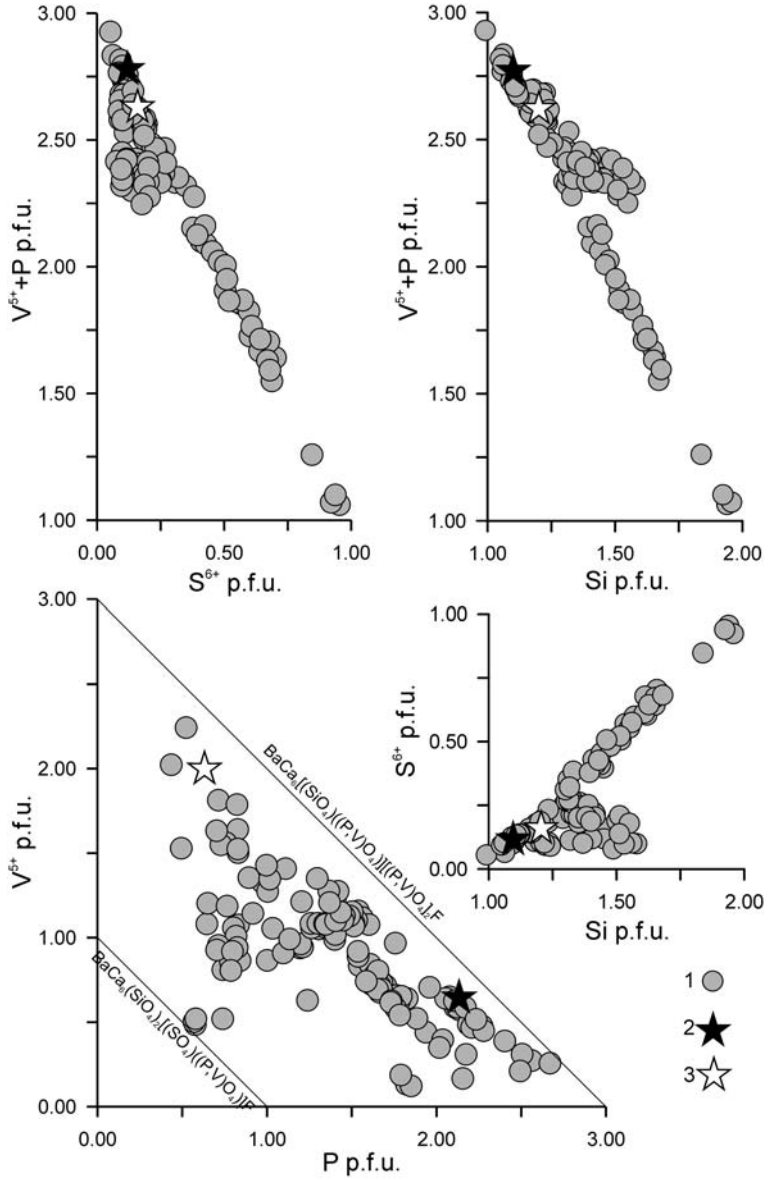

FIG. 5. Correlations S^{6+} + Si *vs.* V + P, P *vs.* V^{5+} and Si *vs.* S constructed from results of EMPA of zadovite-series minerals (1); holotype zadovite (2); and holotype aradite (3).

is situated in the antiperovskite layer at (1/3, 2/3, 0.03) and is occupied by Si and pentavalent cations (P or V) in an Si:(P or V) ratio of 1:1. The overall charge at *T*1 is thus 4.5. The *T*1 atom has three shorter bonds towards *O*2 and one slightly longer bond along the rotation axis towards *O*1. In zadovite the *T*1 site is occupied 1:1 by Si and P while in aradite the corresponding site is occupied by 23.7(13)% V, 26.3% P and 50% Si. Due to their similar scattering power, Si and P could not be distinguished and only the occupancy for V was refined. However, it is reasonable to expect a net charge of 4.5+ at *T*1. Thus 50% is occupied by Si while the occupancy factor for P may be calculated

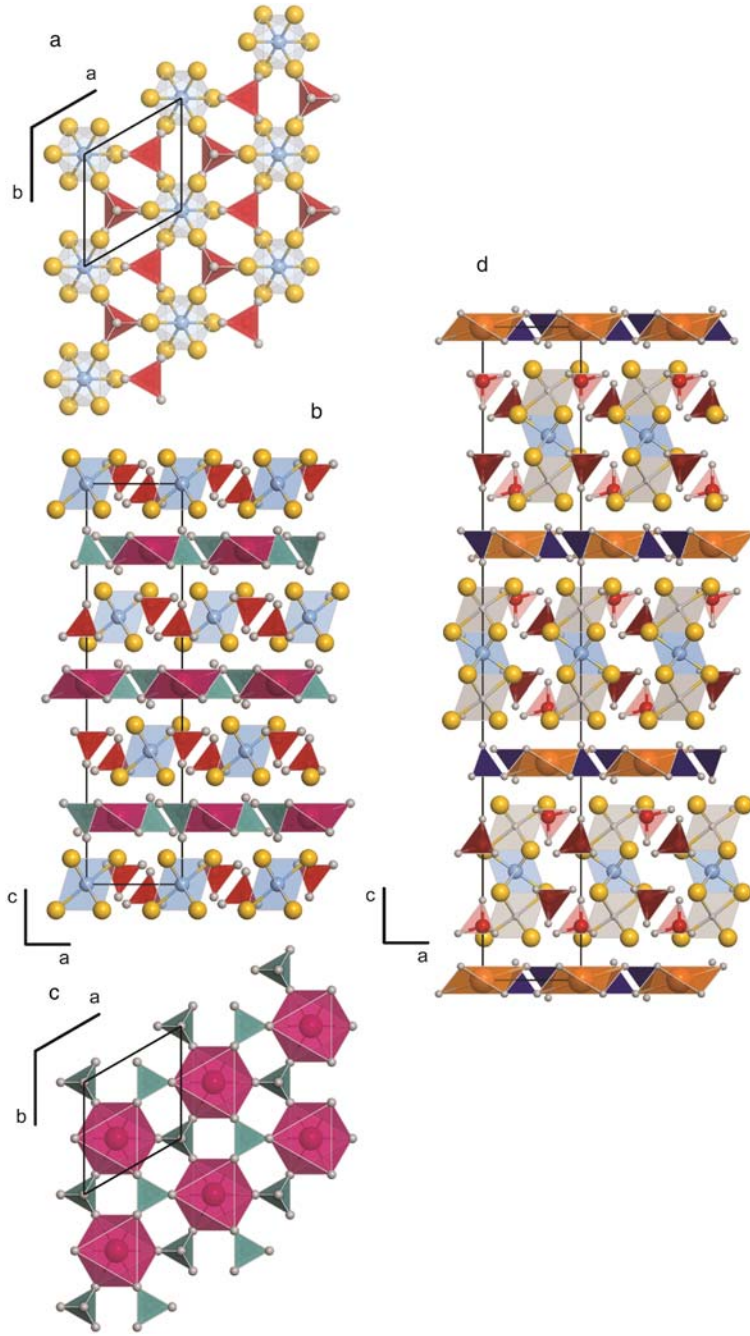

FIG. 6. The crystal structure of the zadovite structure type (*a–c*) is characterized by a 1:1 intercalation (*b*) of an antiperovskite-like $\{[FCa_6](TO_4)_2\}^{4+}$ module (*a*) and $Ba(TO_4)_2^{4-}$ module (*c*) hosting a large cation. The structure is related closely to that of nabimusaite $KCa_{12}(SiO_4)_4(SO_4)_2O_2F$ (*d*). The structure of nabimusaite represents triplets of antiperovkskite-like modules $[Ca_{12}(SiO_4)_4O_2F]^{3+}$ intercalated by a similar module as in the zadovite structure type, but occupied by K and SO_4 tetrahedra ($K(SO_4)_2^{3-}$). Both structures are related to the crystal structure of alite (hatrurite) $Ca_3(SiO_4)O$, which represents a continuous stacking of antiperovskite-like layers.

by difference. Beside the scattering power, this assumption is supported by a rough calculation of the theoretical bond length. For zadovite $T1$–O = 0.5 × 1.55 Å + 0.5 × 1.64 Å = 1.595 Å corresponds to the determined average $T1$–O bond length of 1.600 Å (Table 5). For aradite the assumed tetrahedral cation distribution pattern suggests $T1$–O = 0.237 × 1.73 Å + 0.263 × 1.55 Å + 0.5 × 1.64 Å = 1.638 Å, which fits the measured value of 1.628 Å (Table 5).

The $T2$ site, at (2/3, 1/3, 0.15) belongs to the interlayer and is occupied by pentavalent cations. The $T2$ atom bonds three times to $O3$ while the fourth apex ($O4$) along the threefold axis is slightly longer similar to that observed for the $T1$ tetrahedron. End-member zadovite hosts only P at $T2$ while end-member aradite requires full V occupancy at $T2$. As a matter of fact, both measured single crystals represent complex solid solutions. The zadovite investigated structurally has a refined P:V ratio of 69.5:30.5 while the ratio for aradite is 24.4:75.6. The predicted bond lengths for $T2$–O, 1.60 Å for zadovite, 1.686 Å for aradite, correspond to the measured values 1.596 and 1.678 Å, respectively. The size increase of both tetrahedral sites ($T1$ and $T2$) is the main reason for the increase in the unit-cell parameter c, which is ~2% larger for aradite compared to zadovite (Table 2).

In addition to $T1$, the antiperovskite layer $\{[FCa_6](TO_4)_2\}^{4+}$ contains a regular FCa_6 octahedron with a F–Ca bond length of 2.58 Å and Ca–F–Ca angles of 83° and 97°, respectively, for both zadovite and aradite (Fig. 6). The intercalated Ba $(TO_4)_2^{4-}$ layer hosts a large cation site usually occupied by Ba. The Ba site is coordinated by six $O3$ sites, which form the triangular base of the $T2$ tetrahedron. In aradite the site is fully occupied by Ba; zadovite used for structure refinement has minor Na (1.2(2)%) at the Ba site. There are several ways to maintain the charge balance due to the substitution Na^+ for Ba^{2+}, for example by replacement of (P or V)$^{5+}$ by S^{6+} at one of the two tetrahedral sites, or substitution of Si^{4+} by (P or V)$^{5+}$ at the $T1$ site.

Compared to the related structure type of nabimusaite $KCa_{12}(SiO_4)_4(SO_4)_2O_2F$ (Fig. 6), which is built up by triplets of antiperovskite-like layers intercalated by $K(SO_4)_2^{3-}$, the zadovite structure type follows a 1:1 repetition of antiperovskite modules intercalated by $Ba(TO_4)_2^{4-}$ modules (Fig. 6). Both structures are related closely to the structure of the important cement clinker phase 'alite', Ca_3SiO_5, which has been described as the mineral hatrurite (Gross, 1977). The structure of hatrurite (Jeffery, 1952) is represented by a continuous stacking of antiperovskite-like modules along [001] whereby all tetrahedra point to the same direction along [001] in contrast to the 1:1 up, down orientation of the tetrahedra in the antiperovskite modules of the zadovite and nabimusaite structures.

Wide variations of substitutions for tetrahedral cations (Si, P, V, S and Al) in zadovite and aradite indicate a high probability of additional new minerals in this group and also suggest chemical pathways for the synthesis of new advanced materials.

Acknowledgements

Investigations were partially supported by the National Sciences Centre (NCN) of Poland by decision no. 2013/11/B/ST10/00272 (I.G. and E.G.). The authors thank Stuart Mills, Peter Leverett and the anonymous reviewers for their careful reviews which helped to improve a previous version of the manuscript.

References

Bentor, Y.K. (editor) (1960) *Lexique Stratigraphique International, Asie. Volume III, Section 10.2., Israel.* Centre National de la Research Scientifique, Paris.

Britvin, S.N., Vapnik, Y., Polekhovsky, Y.S. and Krivovichev, S.V. (2013*a*) Murashkoite, IMA 2012-071. CNMNC Newsletter No. 15, February 2013, page 8; *Mineralogical Magazine*, **77**, 1–12.

Britvin, S.N., Murashko, M., Vapnik, Y., Polekhovsky, Y. S. and Krivovichev, S.V. (2013*b*) Negevite, IMA 2013–104. CNMNC Newsletter No. 19, February 2014, page 166; *Mineralogical Magazine*, **78**, 165–170.

Britvin, S.N., Murashko, M., Vapnik, Y., Polekhovsky, Y. S. and Krivovichev, S.V. (2013*c*) Halamishite, IMA 2013-105. CNMNC Newsletter No. 19, February 2014, page 166; *Mineralogical Magazine*, **78**, 165–170.

Britvin, S.N., Murashko, M., Vapnik, Y., Polekhovsky, Y. S. and Krivovichev, S.V. (2013*d*) Transjordanite, IMA 2013-106. CNMNC Newsletter No. 19, February 2014, page 166; *Mineralogical Magazine*, **78**, 165–170.

Britvin, S.N., Murashko, M., Vapnik, Y., Polekhovsky, Y. S. and Krivovichev, S.V. (2013*e*) Zuktamrurite, IMA 2013-107. CNMNC Newsletter No. 19, February 2014, page 166; *Mineralogical Magazine*, **78**, 165–170.

Comodi, L, Liu, Y., Stoppa, F. and Woolley, A.R. (1999) A multi-method analysis of Si-, S- and REE-rich apatite from a new find of kalsilite-bearing leucitite (Abruzzi, Italy). *Mineralogical Magazine*, **63**, 661–672.

Dickens, B. and Brown W.E. (1971) The crystal structure of $Ca_5(PO_4)2SiO_4$ (silico-carnotite). *Tschermaks Mineralogische und Petrographische Mitteilungen*, **16**, 1–27.

Fayos, J., Glasser, F.P., Howie, R.A., Lachowski, E. and Perez-Mendez, M. (1985) Structure of dodecacalcium potassium fluoride dioxide terasilicate bis (sulphate), $KF.2[Ca_6(SO_4)(SiO_4)_2O]$: a fluorine-containing phase encountered in cement clinker production process. *Acta Crystallographica*, **C41**, 814–816.

Ferraris, G., Makovicky, E. and Merlino, S. (2008) *Crystallography of Modular Materials.* Oxford University Press, New York.

Frost, R.L., Weier, M.L. and Stuart, M.J. (2007) A vibrational spectroscopic study of perhamite, an unusual silico-phosphate. *Spectrochimica Acta Part A: Molecular and Biomolecular Spectroscopy*, **67**, 604–610.

Frost, R.L., Palmer, S.J., Cejka, J., Sejkora, J., Pláśil, J., Bahfennea, S. and Keeffea, E.C.A (2011) Raman spectroscopic study of the different vanadate groups in solid-state compounds – model case:mineral phases vésigniéite $[BaCu_3(VO_4)_2(OH)_2]$ and volborthite $[Cu_3V_2O_7(OH)_2{\cdot}2H_2O]$. *Journal of Raman Spectroscopy*, **42**, 1701–1710.

Galuskin, E.V., Galuskina, I.O., Kusz, J. Armbruster, T., Marzec, K.M., Dzierżanowski, P. and Murashko, M. (2014) Vapnikite Ca_3UO_6 – a new double-perovskite mineral from pyrometamorphic larnite rocks of the Jabel Harmun, Palestinian Autonomy, Israel. *Mineralogical Magazine*, **78**, 571–581.

Galuskin, E.V., Gfeller, F., Armbruster, T., Galuskina, I. O.,Vapnik, Y., Dulski, M., Murashko, M., Dzierżanowski, P., Sharygin, V.V., Krivovichev, S.V. and Wirth, R. (2015*a*) Mayenite supergroup, Part III: Fluormayenite, $Ca_{12}Al_{14}O_{32}$ $[\square 4F_2]$, and fluorkyuygenite, $Ca_{12}Al_{14}O_{32}[(H_2O)_4F_2]$, two new minerals of mayenite supergroup from pyrometamorphic rock of Hatrurim Complex. *European Journal Mineralogy*, **27**, 123–126.

Galuskin, E.V., Gfeller, F., Armbruster, T., Galuskina, I. O., Vapnik, Ye., Murashko, M., Wodyka, R. and Dzierżanowski, P. (2015*b*) New minerals with modular structure derived from hatrurite from the pyrometamorphic Hatrurim Complex, Part I: Nabimusaite, $KCa_{12}(SiO_4)_4(SO_4)_2O_2F$, from larnite rock of the Jabel Harmun, Palestinian Autonomy, Israel. *Mineralogical Magazine*, **79**, 1061–1072.

Galuskina, I.O., Vapnik, Y., Prusik, K., Dzierżanowski, P., Murashko, M. and Galuskin, E.V. (2013) Gurimite, IMA 2013-032. CNMNC Newsletter No. 16, August 2013, page 2708; *Mineralogical Magazine*, **77**, 2695–2709.

Galuskina, I.O., Galuskin, E.V., Pakhomova, A.S., Widmer, R., Armbruster, T., Lazic, B., Grew, E.S., Vapnik, Y., Dzierżanowski, P. and Murashko, M. (2014*a*) Khesinite, IMA 2014-033. CNMNC Newsletter No. 21, August 2014, page 802; *Mineralogical Magazine*, **78**, 797–804.

Galuskina, I.O., Vapnik, Y., Lazic, B., Armbruster, T., Murashko, M. and Galuskin, E.V. (2014*b*) Harmunite $CaFe_2O_4$ – a new mineral from the Jabel Harmun, West Bank, Palestinian Autonomy, Israel. *American Mineralogist*, **99**, 965–975.

Galuskina, I.O., Vapnik, Y., Lazic, B., Armbruster, T., Murashko, M. and Galuskin, E.V. (2014c) Dzierżanowskite, IMA 2014-032. CNMNC Newsletter No. 21, August 2014, page 802; *Mineralogical Magazine*, **78**, 797–804.

Geller, Y.I., Burg, A., Halicz, L. and Kolodny, Y. (2012) System closure during the combustion metamorphic "Mottled Zone" event, Israel. *Chemical Geology*, **334**, 25–36.

Gfeller, F., Widmer, R., Krüger, B., Galuskin, E.V., Galuskina, I.O. and Armbruster, T. (2015) The crystal structure of flamite and its relation to Ca_2SiO_4 polymorphs and nagelschmidtite. *European Journal of Mineralogy*, **27**, DOI: 10.1127/ejm/2015/0027-2476.

Gross, S. (1977) The mineralogy of the Hatrurim Formation, Israel. *Geological Survey of Israel Bulletin*, **70**, 1–80.

Irran, E., Tillmanns, E. and Hentschel, G. (1997) Ternesite, $Ca_5(SiO_4)_2SO_4$, a new mineral from the Ettringer Bellerberg/Eifel, Germany. *Mineralogy and Petrology*, **60**, 121–132.

Jeffery, J.W. (1952) The crystal structure of tricalcium silicate. *Acta Crystallographica*, **5**, 26–35.

Matthews, A. and Gross, S. (1980) Petrologic evolution of the Mottled Zone (Hatrurim) metamorphic complex of Israel. *Israel Journal of Earth Sciences*, **29**, 93–106.

Mumme, W., Hill, R., Bushnell-Wye, G. and Segnit, E. (1995) Rietveld crystal structure refinements, crystal chemistry and calculated powder diffraction data for the polymorphs of dicalcium silicate and related phases. *Neues Jahrbuch für Mineralogie, Abhandlungen*, **169**, 35–68.

Murashko, M.N., Chukanov, N.V., Mukhanova, A.A., Vapnik, E., Britvin, S.N., Krivovichev, S.V., Polekhovsky, Y.S. and Ivakin, Y.D. (2010) Barioferrite $BaFe^{3+}_{12}O_{19}$ – a new magnetoplumbitegroup mineral from Hatrurim Formation, Israel. *Zapiski Rossiyskogo Mineralogicheskogo Obshchestva*, **139**, 22–31.

Novikov, I., Vapnik, Y. and Safonova, I. (2013) Mud volcano origin of the Mottled Zone, South Levant. *Geoscience Frontiers*, **4**, 597–619.

Saalfeld, H. and Klaska, K. (1981) The crystal structure of $6Ca_2SiO_4{\cdot}1Ca_3(PO_4)$. *Zeitschrift für Kristallographie*, **155**, 65–73.

Schindler, M., Hawthorne, F.C. and Baur, W.H. (2000) Crystal chemical aspects of vanadium: polyhedral

geometries, characteristic bond valences, and polymerization of (VOn) polyhedra. *Chemistry Materials*, **12**, 1248–1259.

Seryotkin, Y.V., Sokol, E.V. and Kokh, S. (2012) Natural pseudowollastonite: crystal structure, associated minerals, and geological context. *Lithos*, **134–135**, 75–90.

Shannon, R.D. (1976) Revised effective ionic radii and systematic studies of interatomic distances in halides and chalcogenides. *Acta Crystallographica*, **A32**, 751–767.

Sharygin, V.V., Lazic, B., Armbruster, T.M., Murashko, M.N., Wirth, R., Galuskina, I.O., Galuskin, E.V., Vapnik, Y., Britvin, S.N. and Logvinova, A.M. (2013) Shulamitite $Ca_3TiFe^{3+}AlO_8$ – A new perovskite-related mineral from Hatrurim Basin, Israel. *European Journal of Mineralogy*, **25**, 97–111.

Sokol, E.V., Novikov, I.S., Vapnik, Y. and Sharygin, V.V. (2007) Gas fire from mud volcanoes as a trigger for the appearance of high-temperature pyrometamorphic rocks of the Hatrurim Formation (Dead Sea area). *Doklady Earth Sciences*, **413A**, 474–480.

Sokol, E.V., Novikov, I.S., Zateeva, S.N., Sharygin, V.V. and Vapnik, Y. (2008) Pyrometamorphic rocks of the spurrite–merwinite facies as indicators of hydrocarbon discharge zones (the Hatrurim Formation, Israel). *Doklady Earth Sciences*, **420**, 608–614.

Sokol, E.V., Seryotkin, Y.V., Kokh, S.N., Vapnik, Y., Nigmatulina, E.N., Goryainov, S.V., Belogub, E.V. and Sharygin, V.V. (2014) Flamite, IMA 2013-122. CNMNC Newsletter No. 20, June 2014, page 550; *Mineralogical Magazine*, **78**, 549–558.

Sokolova, E.V., Yamnova, N.A., Egorov-Tismenko, Y.K. and Khomyakov, A.P. (1984) The crystal structure of a new sodium-calcium-barium phosphate of Na, Ca and Ba $(Na_5Ca)Ca_6Ba(PO_4)_6F_3$. *Doklady Akademii Nauk SSSR*, **274**, 78–83.

Vapnik, Y., Sokol, E., Murashko, M. and Sharygin, V. (2006) The enigma of Hatrurim. *Mineralogical Almanac*, **10**, 69–77.